CHINESE OPTICS LETTERS

Vol. 20, No. 7 | July 2022

Probing fluorescence quantum efficiency of single molecules in an organic matrix by monitoring lifetime change during sublimation

Penglong Ren (任鹏龙)[1,2], Shangming Wei (韦尚明)[1,2], Pu Zhang (张 朴)[1,2], and Xue-Wen Chen (陈学文)[1,2*]

[1] School of Physics and Wuhan National Laboratory for Optoelectronics, Huazhong University of Science and Technology, Wuhan 430074, China

[2] Institute for Quantum Science and Engineering, Huazhong University of Science and Technology, Wuhan 430074, China

*Corresponding author: xuewen_chen@hust.edu.cn

Received January 17, 2022 | Accepted April 14, 2022 | Posted Online May 4, 2022

Quantum efficiency is a critical piece of information of a quantum emitter and regulates the emitter's fluorescence decay dynamics in an optical environment through the Purcell effect. Here, we present a simple way to experimentally probe fluorescence quantum efficiency of single dibenzoterrylene molecules embedded in a thin anthracene microcrystal obtained through a co-sublimation process. In particular, we correlate the fluorescence lifetime change of single dibenzoterrylene molecules with the variation of the matrix thickness due to natural sublimation. With the identification of the molecule emission dipole orientation, we could deduce the near-unity intrinsic quantum efficiency of dibenzoterrylene molecules in the anthracene matrix.

Keywords: quantum emitter; single-molecule spectroscopy; quantum efficiency; single-photon source.
DOI: 10.3788/COL202220.073602

1. Introduction

Organic molecules are attractive to both physicists and chemists because molecules could have high quantum efficiencies in light emission and be chemically synthesized to have transitions at desired wavelengths. In the past several decades, single molecules embedded in solids, as isolated individual quantum systems, have become an attractive class of sources of single photons since a single two-level system cannot emit two photons simultaneously, as each excitation and emission cycle requires a finite time[1,2]. Single photons are one of the key building blocks for photonic quantum technologies, such as quantum computation, quantum key distribution, and metrology[2–6]. Compared to various other solid-state single-photon emitters such as self-assembled quantum dots[7–9], color centers in diamond[10–12], and defects in two-dimensional materials[13], single molecules possess several unique properties including small size of about one nanometer (suitable for high-density doping), flexibility in the synthesis, and strong and stable Fourier-transform-limited zero-phonon lines at low temperature. In particular, 7,8:15,16-dibenzoterrylene (DBT) molecules embedded in anthracene (AC) have been actively studied as definitely stable single-photon emitters with nonblinking emission[13–16] and lifetime-limited linewidth[17–19]. Recent reports have explored the integration of single DBT molecules with planar photonic circuits[15,20–23]. However, despite enormous studies, the quantum efficiency of single DBT molecules in the AC matrix, as a critical piece of information, has not been experimentally measured.

The quantum efficiency of an emitter indicates the ability to emit a photon once an excitation photon is absorbed and is defined as $\eta = \Gamma_r/(\Gamma_r + \Gamma_{nr})$, where Γ_r and Γ_{nr} are the radiative decay rate and nonradiative decay rate of the emitter, respectively. While the theoretical definition of quantum efficiency is crystal clear, its experimental measurement is highly nontrivial. In the past two decades, there have been several experiments reporting the measurements of absolute quantum efficiency of single emitters[24–28]. The existing applied methods can be classified into two types, i.e., (i) studying the emitter's decay rate with nano-controlled variation of the optical environment[24–27] and (ii) measuring the saturation of the emission of the emitter with pre-characterized total detection efficiency of the system[28]. The first approach relies on the Purcell effect[29–31] and requires a stabilized nanometer-resolution control of the spatial arrangement of the emitter with respect to a photonic structure, which is technically challenging and tedious. The second approach has the difficulty in determining the total detection efficiency for the fluorescence by taking into account the collection efficiency of the first lens and the subsequent loss of each element in the system. Both approaches are difficult to

implement for DBT molecules in AC crystal, and thus their quantum efficiencies have not been measured at the single-molecule level.

In this work, we present a simple method to experimentally probe fluorescence quantum efficiency of single DBT molecules embedded in AC microcrystal by monitoring the fluorescence lifetime change during the process of natural sublimation. The decrease of the thickness of the microcrystal due to sublimation induces the change of the optical environment of the molecules and, consequently, the change of the Purcell factor or the local density of optical states (LDOS), which manifests through the modification of the fluorescence lifetime[30]. To correlate the lifetime change with the quantum efficiency, we identify the orientation of the molecule's emission dipole from the radiation pattern through the back-focal-plane (BFP) imaging and measure the thickness of the microcrystal via atomic force microscope (AFM). Based on a series of measured crystal thicknesses and lifetimes recorded on the same molecules, we could deduce the intrinsic quantum efficiencies of single DBT molecules in AC microcrystal.

2. Experiments

DBT-doped AC (DBT:AC) microcrystals with preset concentrations are prepared through a co-sublimation process[16,17]. Good mechanical rigidity allows us to use a tapered fiber tip to pick up and transfer the microcrystal to a coverslip for further characterization and spectroscopic study. As sketched in Fig. 1(a), a home-built confocal microscope combined with AFM provides access to a wide range of optical measurements, including confocal scan fluorescence imaging, second-order photon correlation function $g^{(2)}(\tau)$, photoluminescence (PL) decay dynamics, BFP imaging, and sample topographic study. The excitation laser sources are a continuous wave (CW) laser (Matisse 2TS, Spectra-Physics) and a pulse laser (pulse width 30 ps, NKT EXTREME EXR-20), and both are set at 730 nm with a band-pass filter with a 10 nm bandwidth. The polarization state of the excitation is first purified by a polarizer (POL) and then controlled through a half-wave plate (HWP) to match the dipole orientation of DBT molecules embedded in AC microcrystal. After a nonpolarizing cube beamsplitter (BS) with a splitting ratio of 30:70 (R:T), the excitation light is focused onto the sample by an oil-immersion objective of numerical aperture NA = 1.35. The fluorescence from the excited molecule will be collected with the same objective. The sample is mounted on a 3D piezo-electric stage to realize two-dimensional positioning or scanning with respect to the laser beam and flexible adjustment of the focus in the axial direction. The collected fluorescence successively passes through a long-pass filter (LP) with a cut-off wavelength at 750 nm and a spatial filtering module including two lenses (L1, L2) and a pinhole on the real image plane (PH-R) for camera imaging and photon counting. The flip mirror (FM) allows us to image the fluorescence (real/BFP) of single DBTs with a camera if the FM is flipped in and to do single-photon counting measurement if the FM is out. Our Hanbury-

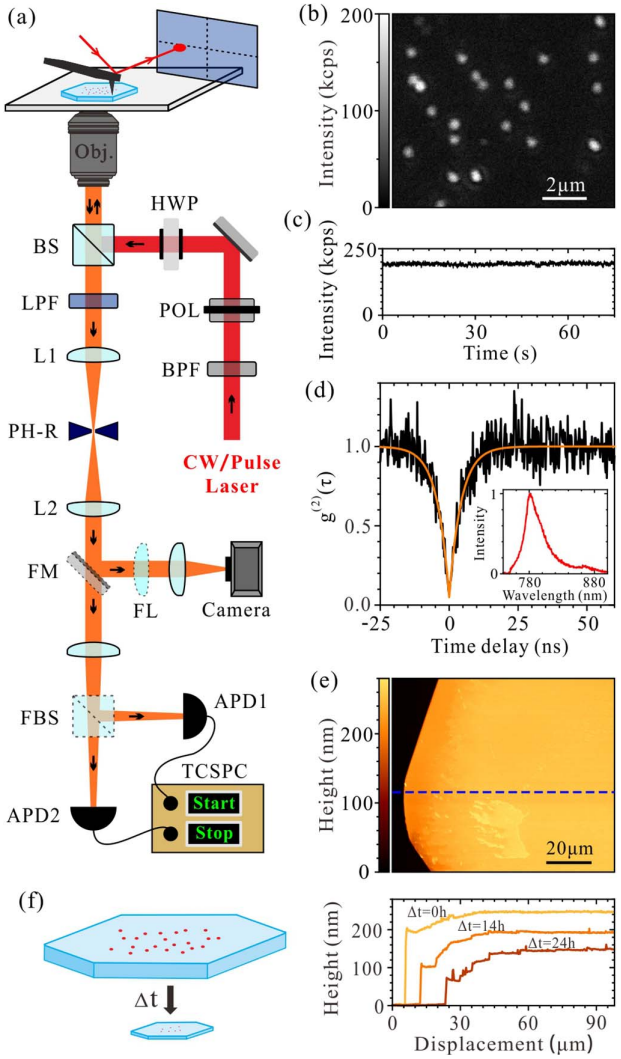

Fig. 1. (a) Sketch of the experimental setup (see text for details). (b) Fluorescence image of single dibenzoterrylene (DBT) molecules embedded in an anthracene (AC) microcrystal obtained through confocal scanning; (c) photoluminescence (PL) time trace and (d) normalized second-order photon correlation function of fluorescence from a DBT molecule. The inset in (d) is the emission spectrum of the same molecule. (e) Atomic force microscope (AFM) topographic image of a part of an AC microcrystal. (f) Left: schematic illustration of the sublimation process of the AC microcrystal; right: cross-sectional plots of the height along the same blue dashed line shown in (e) at different times, which demonstrate the sublimation process.

Brown and Twiss (HBT) setup comprises a 50:50 flippable BS (FBS) and two avalanche photodiodes (APDs; SPCM-AQRH-14, Excelitas Technologies). The photon detection events recorded from two APDs are analyzed by the time-correlated single-photon counting (TCSPC) unit (Picoharp 300, PicoQuant) and give $g^{(2)}(\tau)$ of a single molecule. We can also take off the FBS, and then all photons can be detected by APD2, which is the usual configuration used in the fluorescence confocal scan and PL decay dynamics study. For the PL decay lifetime measurement, molecules will be excited by the pulse laser with a 2.1 MHz repetition rate.

3. Results

Figure 1(b) shows a confocal-scanning fluorescence image of single DBT molecules embedded in an AC microcrystal in a small region under CW laser excitation at a wavelength of 730 nm. Each molecule is spatially well separated and indicates a proper concentration of molecules in the sample. Figures 1(c) and 1(d) present a recorded PL time trace and normalized second-order photon correlation function $g^{(2)}(\tau)$ from the same molecule. The nonblinking fluorescence has a count rate of about 190 kcps (cps, counts per second) with a background rate of 1 kcps. The $g^{(2)}(\tau)$ curve exhibits a pronounced antibunching dip of 0.05 ± 0.03 at zero time delay. The inset of Fig. 1(d) is the emission spectrum of the molecule. These results confirm that the individual DBT molecule inside the AC microcrystal has stable and pure single-photon emission. The crystalline DBT:AC microcrystal has flat surface, which is shown via an AFM topography image in Fig. 1(e). As sketched in Fig. 1(f), when the microcrystal is exposed in the air, sublimation brings decreasing thickness of the AC crystal, which is indicated by cross-sectional plots of the height along the blue dashed line in Fig. 1(e).

The structure of the sample we measured is depicted in Fig. 2(a), where H represents the thickness of the AC microcrystal, and h is the height of the molecule above the glass coverslip. As illustrated in Fig. 2(a), the emission dipole moment of the DBT molecule is aligned with the b axis of the crystal[32]. The orientation has been confirmed by the consistency between the measured and simulated BFP emission patterns in Fig. 2(b). Since the insertion site of a DBT molecule embedded in AC is stable during the sublimation of the microcrystal in air[32], the distance from the emitter to the AC-air interface gradually decreases over time, and the LDOS experienced by the emitter correspondingly changes. Therefore, the natural sublimation of the DBT:AC microcrystal offers a simple method for altering the LDOS. Subsequently, the radiative decay rate $\Gamma_r \propto$ LDOS and, in turn, the fluorescence lifetime of the molecule $\tau = 1/(\Gamma_r + \Gamma_{nr})$ vary during the sublimation. We continuously performed lifetime measurements for the target DBT molecule #1 and AFM topographic imaging for the AC microcrystal to measure its thickness. A series of the lifetime measurement results are shown in Figs. 2(c)–2(f). The insets display the corresponding regional AFM topographic images of the microcrystal, where the location of DBT molecule #1 is marked with a red star. It is clearly observed that crystal thickness decreases, and the lifetime of the molecule increases during the sublimation.

Two different DBT molecules, molecule #1 and another labeled as molecule #2, are then studied in comparison. The crystal thickness-dependent total decay rates (Γ) of the molecules are obtained from the measured lifetimes ($\tau = 1/\Gamma$) and shown in Fig. 3(a). The total decay rate can be expressed with $\Gamma = \Gamma_r + \Gamma_{nr}$, as contributed by the radiative and nonradiative decay rates. We observed that the two molecules still survived and were producing stable fluorescence emission even 4 h after the AFM scans and lifetime measurements were finished. At that time, the crystal thickness should have been further reduced by tens of nanometers due to sublimation. Therefore, the target molecules must be buried deep down below the top surface of the crystal, and the nonradiative decay rates Γ_{nr} can be regarded as constant during the sublimation. So, the decrease of the total decay rates stems from the change in the radiative decay rates related to the LDOS. We describe the LDOS with the Purcell factor F_P, which is by definition Γ_r/Γ_r^0 and can be numerically determined as the ratio between radiated powers of a classical dipole (Chap. 8 of Ref. [33]), i.e.,

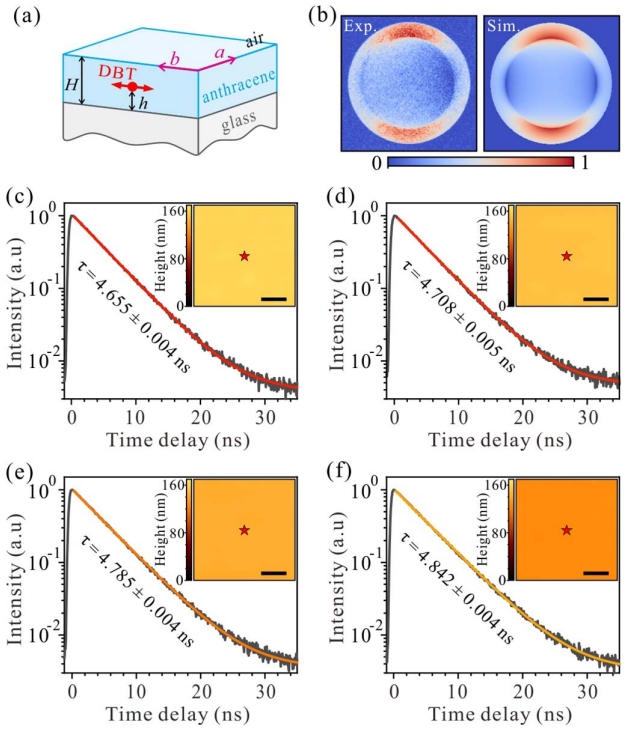

Fig. 2. (a) Schematic diagram of the sample structure. (b) Measured and simulated back-focal plane (BFP) images of the emission from a single molecule oriented along the b axis of the AC microcrystal. (c)–(f) Measured and fitted PL decay curves from the same DBT molecule at different times. Insets: AFM topographic images of the region of the AC microcrystal where the molecule is located. The red star marks the location of the measured molecule. Scale bar: 500 nm.

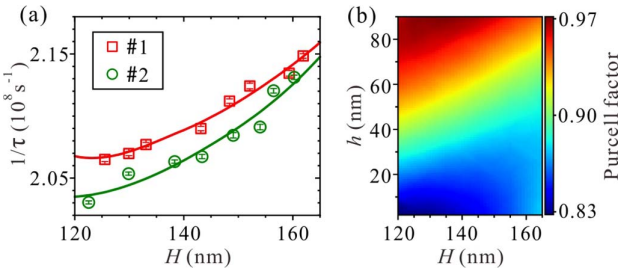

Fig. 3. (a) Measured and fitted total decay rates ($1/\tau$) of two different DBT molecules as functions of the AC microcrystal thicknesses. (b) Purcell factor distribution versus emitter dipole position h and the microcrystal thickness H.

$$F_P = \frac{\Gamma_r}{\Gamma_r^0} = \frac{P}{P_0}. \quad (1)$$

Here, Γ_r^0 is the radiative decay rate of a DBT molecule in unbounded AC crystal. P and P_0 are, respectively, the radiated powers of a classical dipole mimicking the DBT molecule in the AC microcrystal and unbounded AC crystal environment. Then, we calculated the two powers in the frequency domain with finite-element method based COMSOL Multiphysics. The computational domain containing the dipole and dielectric environment is truncated with perfectly matched layers to absorb outgoing waves and discretized with nonuniform tetrahedral meshes optimized to guarantee convergence. The dipole is aligned to the b axis and working at the wavelength of 781 nm. The anisotropy of the AC crystal has been taken into account in the simulation as $n_x = 1.55$, $n_y = 1.75$, $n_z = 2.05$[34]. For glass and air, $n_{\text{glass}} = 1.52$ and $n_{\text{air}} = 1$. In our case, the Purcell factor $F_P(H,h)$ is a function of the crystal thickness H and emitter position h. The two parameters were swept in certain ranges, and the resulting $F_P(H,h)$ is shown in Fig. 3(b). When the emitter is located close to the glass coverslip, we clearly see F_P increases with the crystal thickness H. The trend is consistent with the results shown in Fig. 3(a). The radiative decay rate can be expressed as $\Gamma_r(H,h) = \Gamma_r^0 F_P(H,h)$, and thus we can express the total decay rate Γ as

$$\Gamma(H,h) = \Gamma_r^0 F_P(H,h) + \Gamma_{nr}. \quad (2)$$

During the sublimation, the position h of a specific molecule remains unchanged. Thus, the measured lifetime $\tau(H)$ is only a function of H. Using the intrinsic quantum efficiency defined by $\eta_0 = \Gamma_r^0/(\Gamma_r^0 + \Gamma_{nr})$, we can rewrite Eq. (2) as

$$\frac{1}{\tau(H)} = \Gamma_r^0 F_P(H,h) + \Gamma_r^0\left(\frac{1}{\eta_0} - 1\right). \quad (3)$$

Equation (3) provides a model to explain the sublimation-induced lifetime change. The unknown parameters η, Γ_r^0, and h can be further extracted by fitting the model to the measured lifetimes at different crystal thicknesses. When we stopped the lifetime measurements, the crystal still had a thickness of 120 nm. Considering that the measured molecules are buried deep down below the top surface, the emitter position h should be fitted in a range from 0 nm to 90 nm, which is consistent with the h range of the $F_P(H,h)$ map in Fig. 3(b). According to the simulated $F_P(H,h)$, we find the best fitted set of η, Γ_r^0, and h, which minimizes the residual error between theoretical calculation based on Eq. (3) and measured lifetime data. The fitted results are plotted in Fig. 3(a). For molecule #1, we find $7\,\text{nm} < h < 12\,\text{nm}$, $93\% < \eta_0 < 100\%$, and $\Gamma_r^0 = (2.48 \pm 0.21) \times 10^8\ \text{s}^{-1}$; for molecule #2, $0\,\text{nm} < h < 4\,\text{nm}$, $88\% < \eta_0 < 100\%$, and $\Gamma_r^0 = (2.42 \pm 0.33) \times 10^8\ \text{s}^{-1}$. The average intrinsic quantum efficiency of 95% agrees with the reported near-unity values for DBT molecules at the ensemble level at low temperature[35].

4. Discussion

We utilized the natural sublimation of the AC microcrystal, which induces optical environment change for embedded DBT molecules and experimentally probed fluorescence quantum efficiency of single DBT molecules by monitoring the fluorescence lifetime change due to the optical environment variation. By identifying the orientation of the molecule emission dipole from the radiation pattern through BFP imaging, we established a Purcell factor distribution as a function of crystal thickness and molecule position to describe the sublimation-induced lifetime change and analyze the quantum efficiency. Based on a series of measured AC crystal thicknesses and lifetimes recorded on the same molecules, we deduced the near-unity intrinsic quantum efficiency of the DBT molecule in the AC microcrystal.

Acknowledgement

This work was supported by the National Natural Science Foundation of China (No. 11874166). P. Ren thanks J. Tang for useful discussion.

References

1. T. Basché, W. Moerner, M. Orrit, and U. Wild, *Single-Molecule Optical Detection, Imaging and Spectroscopy* (VCH, 1997).
2. B. Lounis and M. Orrit, "Single-photon sources," Rep. Prog. Phys. **68**, 1129 (2005).
3. P. Kok, W. J. Munro, K. Nemoto, T. C. Ralph, J. P. Dowling, and G. J. Milburn, "Linear optical quantum computing with photonic qubits," Rev. Mod. Phys. **79**, 135 (2007).
4. S. Scheel, "Single-photon sources–an introduction," J. Mod. Opt. **56**, 141 (2009).
5. S. V. Polyakov and A. L. Migdall, "Quantum radiometry," J. Mod. Opt. **56**, 1045 (2009).
6. P. Zhang, L. Lu, F. Qu, X. Jiang, X. Zheng, Y. Lu, S. Zhu, and X.-S. Ma, "High-quality quantum process tomography of time-bin qubit's transmission over a metropolitan fiber network and its application," Chin. Opt. Lett. **18**, 082701 (2020).
7. P. Michler, A. Kiraz, C. Becher, W. V. Schoenfeld, P. M. Petroff, L. Zhang, E. Hu, and A. Imamoglu, "A quantum dot single-photon turnstile device," Science **290**, 2282 (2000).
8. J. C. Loredo, N. A. Zakaria, N. Somaschi, C. Anton, L. de Santis, V. Giesz, T. Grange, M. A. Broome, O. Gazzano, G. Coppola, I. Sagnes, A. Lemaitre, A. Auffeves, P. Senellart, M. P. Almeida, and A. G. White, "Scalable performance in solid-state single-photon sources," Optica **3**, 433 (2016).
9. X. Ding, Y. He, Z. C. Duan, N. Gregersen, M. C. Chen, S. Unsleber, S. Maier, C. Schneider, M. Kamp, S. Höfling, C.-Y. Lu, and J.-W. Pan, "On-demand single photons with high extraction efficiency and near-unity indistinguishability from a resonantly driven quantum dot in a micropillar," Phys. Rev. Lett. **116**, 020401 (2016).
10. I. Aharonovich, S. Castelletto, D. A. Simpson, C. H. Su, A. D. Greentree, and S. Prawer, "Diamond-based single-photon emitters," Rep. Prog. Phys. **74**, 076501 (2011).
11. I. Aharonovich, S. Castelletto, D. A. Simpson, C. H. Su, A. D. Greentree, and S. Prawer, "Diamond-based single-photon emitters," Rep. Prog. Phys. **74**, 076501 (2011).
12. B. Zhao, Y. Dong, S. Zhang, X. Chen, W. Zhu, and F. Sun, "Improving the NV generation efficiency by electron irradiation," Chin. Opt. Lett. **18**, 080201 (2020).

13. J. Hong, C. Jin, J. Yuan, and Z. Zhang, "Atomic defects in two-dimensional materials: from single-atom spectroscopy to functionalities in opto-/electronics, nanomagnetism, and catalysis," Adv. Mater. **29**, 1606434 (2017).
14. C. Toninelli, K. Early, J. Bremi, A. Renn, S. Götzinger, and V. Sandoghdar, "Near-infrared single-photons from aligned molecules in ultrathin crystalline films at room temperature," Opt. Express **18**, 6577 (2010).
15. C. Polisseni, K. D. Major, S. Boissier, S. Grandi, A. S. Clark, and E. A. Hinds, "Stable, single-photon emitter in a thin organic crystal for application to quantum-photonic devices," Opt. Express **24**, 5615 (2016).
16. S. Wei, P. Ren, Y. He, P. Zhang, and X.-W. Chen, "Single-molecule-doped crystalline nanosheets for delicate photophysics studies and directional single-photon-emitting devices," Phys. Rev. Appl **13**, 064023 (2020).
17. A. A. Nicolet, C. Hofmann, M. A. Kol'chenko, B. Kozankiewicz, and M. Orrit, "Single dibenzoterrylene molecules in an anthracene crystal: spectroscopy and photophysics," ChemPhysChem **8**, 1215 (2007).
18. D. Wang, H. Kelkar, D. Martin-Cano, T. Utikal, S. Götzinger, and V. Sandoghdar, "Coherent coupling of a single molecule to a scanning Fabry–Perot microcavity," Phys. Rev. X **7**, 021014 (2017).
19. S. Pazzagli, P. Lombardi, D. Martella, M. Colautti, B. Tiribilli, F. S. Cataliotti, and C. Toninelli, "Self-assembled nanocrystals of polycyclic aromatic hydrocarbons show photostable single-photon emission," ACS Nano **12**, 4295 (2018).
20. J. Hwang and E. A. Hinds, "Dye molecules as single-photon sources and large optical nonlinearities on a chip," New J. Phys. **13**, 085009 (2011).
21. S. Grandi, M. P. Nielsen, J. Cambiasso, S. Boissier, K. D. Major, C. Reardon, T. F. Krauss, R. F. Oulton, E. A. Hinds, and A. S. Clark, "Hybrid plasmonic waveguide coupling of photons from a single molecule," APL Photonics **4**, 086101 (2019).
22. P. Türschmann, N. Rotenberg, J. Renger, I. Harder, O. Lohse, T. Utikal, S. Götzinger, and V. Sandoghdar, "Chip-based all-optical control of single molecules coherently coupled to a nanoguide," Nano Lett. **17**, 4941 (2017).
23. D. Rattenbacher, A. Shkarin, J. Renger, T. Utikal, S. Götzinger, and V. Sandoghdar, "Coherent coupling of single molecules to on-chip ring resonators," New J. Phys. **21**, 062002 (2019).
24. X. Brokmann, L. Coolen, M. Dahan, and J. P. Hermier, "Measurement of the radiative and nonradiative decay rates of single CdSe nanocrystals through a controlled modification of their spontaneous emission," Phys. Rev. Lett. **93**, 107403 (2004).
25. B. C. Buchler, T. Kalkbrenner, C. Hettich, and V. Sandoghdar, "Measuring the quantum efficiency of the optical emission of single radiating dipoles using a scanning mirror," Phys. Rev. Lett. **95**, 063003 (2005).
26. S. Castelletto, I. Aharonovich, B. C. Gibson, B. C. Johnson, and S. Prawer, "Imaging and quantum-efficiency measurement of chromium emitters in diamond," Phys. Rev. Lett. **105**, 217403 (2010).
27. R. J. Walters, J. Kalkman, A. Polman, H. A. Atwater, and M. J. A. de Dood, "Photoluminescence quantum efficiency of dense silicon nanocrystal ensembles in SiO_2," Phys. Rev. B **73**, 132302 (2006).
28. W. Xu, X. Hou, Y. Meng, R. Meng, Z. Wang, H. Qin, X. Peng, and X.-W. Chen, "Deciphering charging status, absolute quantum efficiency, and absorption cross section of multicarrier states in single colloidal quantum dots," Nano Lett. **17**, 7487 (2017).
29. E. M. Purcell, H. C. Torrey, and R. V. Pound, "Resonance absorption by nuclear magnetic moments in a solid," Phys. Rev. **69**, 37 (1946).
30. W. L. Barnes, "Fluorescence near interfaces: the role of photonic mode density," J. Mod. Opt. **45**, 661 (1998).
31. G. Chen, J. Zhu, and X. Li, "Influence of a dielectric decoupling layer on the local electric field and molecular spectroscopy in plasmonic nanocavities: a numerical study," Chin. Opt. Lett. **19**, 123001 (2021).
32. A. A. Nicolet, P. Bordat, C. Hofmann, M. A. Kol'chenko, B. Kozankiewicz, R. Brown, and M. Orrit, "Single dibenzoterrylene molecules in an anthracene crystal: main insertion sites," ChemPhysChem **8**, 1929 (2007).
33. L. Novotny and B. Hecht, *Principles of Nano-Optics*, 2nd ed. (Cambridge University, 2012).
34. I. Nakada, "The optical properties of anthracene single crystals," J. Phys. Soc. Jpn. **17**, 113 (1962).
35. L. A. Nakhimovsky, I. Joussot-Dubien, and M. Lamotte, *Handbook of Low-Temperature Electronic Spectra of Polycyclic Aromatic Hydrocarbons* (Elsevier, 1989).